Available online at www.sciencedirect.com
SCIENCE DIRECT®
Journal of Nuclear Materials 329–333 (2004) 392–396
journal of nuclear materials
www.elsevier.com/locate/jnucmat

Y_2O_3 nano-particle formation in ODS ferritic steels by Y and O dual ion-implantation

D. Sakuma [a], S. Yamashita [b], K. Oka [a], S. Ohnuki [a,*], L.E. Rehn [c], E. Wakai [d]

[a] *Department of Materials Science, Faculty of Engineering, Graduate School of Engineering, Hokkaido University, N-13, W-8, Kita-ku, Sapporo 060-8628, Japan*
[b] *Oarai Engineering Center, JNC, Oarai, Ibaraki 311-1393, Japan*
[c] *Materials Science Division, Argonne national laboratory, Argonne, IL 60439, USA*
[d] *Japan Atomic Energy Research Institute, Tokai, Ibaraki 319-1195, Japan*

Abstract

For basic understanding of how to produce a homogeneous distribution of nano-scale oxide particles, we have applied dual ion-implantation to make a super-saturation of oxide-forming elements. Y^+ and O^+ ions were implanted into ferritic alloys at room temperature. Both in situ annealing in an electron microscope for thin samples and conventional annealing for bulk samples were carried out at 300–1300 K. Nano-particles of Y_2O_3 precipitated during annealing, where the starting temperatures for the nucleation and growth depended on the annealing methods. In thin specimens the growth and nucleation of Y_2O_3 started at 573 and 613 K. In bulk specimens, the growth and nucleation shifted to higher temperatures. Compared with conventional Mechanical Alloying, it is concluded that dual ion-implantation can produce much finer distributions of nano-scale oxides. In order to explain these results, we emphasize the roles of super-saturated elements and lattice defects.

1. Introduction

Oxide dispersion strengthened (ODS) ferritic steels have excellent resistance to radiation damage, as well as superior high temperature creep strength. From these properties, they are one of the most promising candidate materials for the first wall component in fusion reactors and cladding materials in fast breeder reactors [1–6]. The materials issues for ODS ferritic steels have been the anisotropic mechanical properties due to bamboo structure, stability of oxide particles, heat-treatment condition, chemical composition of minor elements, and others.

New issues are focused on controlling the oxide size and the distribution at the nano-level for developing advanced ODS materials. They are fabricated commercially by mechanical alloying (MA) at ambient temperature, followed by hot-extrusion or hot isostatic pressing (HIP process) around 1150 °C. However, the distribution and size of Y_2O_3 particles are not homogeneous microscopically in the matrix. In order to achieve a homogeneous and nano-scale distribution, it is important to understand the process of atomistic mixing of oxide-forming elements and rearrangement during fabrication.

Recently, important results have been reported on the stability of oxide particles, such as the effectiveness of Ti addition for controlling nano-size oxide particle distributions [7], and high-resolution microscopy showing a faceted interface between the nano-oxide particle and matrix [8]. An important result was reported on high-resolution microscopy of the oxide particles in an ODS austenitic alloy fabricated by conventional MA. The fine particles grew during annealing above 800 °C and showed facetted features similar to precipitates. However, no fine particles were confirmed just after

* Corresponding author. Tel.: +81-11 706 6769; fax: +81-11 706 6772.
E-mail address: ohnuki@loam-ms.eng.hokudai.ac.jp (S. Ohnuki).

0022-3115/$ - see front matter © 2004 Elsevier B.V. All rights reserved.
doi:10.1016/j.jnucmat.2004.04.039

MA. This result suggested that the MA process can induce some super-saturation of oxide-forming elements, which is termed a mechanically forced super-saturation, which can produce precipitation following the HIP process. It is important to control the nano-scale structure of the oxide particles. However, MA the process is not perfect for introducing oxide-forming elements into matrix with nano-scale-dimension. Fortunately, a low temperature ion-implantation provides a method for introducing a homogeneous distribution of the elements in a super-saturated condition.

For this paper, we performed dual ion-implantation and annealing experiments, and evaluated the nano-oxide formation and its distribution in ODS ferritic steels. Specific microstructural changes were surveyed by in situ observation in a high-voltage electron microscope.

2. Experimental

Dual ion-implantation was carried out in the Tandem Facility of Argonne National Laboratory. Both 400 keV Y^+ and 83 keV O^+ ions were implanted at ambient temperature to $1.0\times10^{16}/cm^2$ and $1.5\times10^{16}/cm^2$, respectively. A TRIM96 calculation (Fig. 1) showed a peak predicted implantation at ~80 nm from the surface.

For preparing thin TEM specimens of the implanted layer, we used the following sectioning method. After measuring the polishing rate, a surface layer of ~50 nm was removed by using a polishing in the electrolyte of CH_3COOH:HCl = 19:1, where the optimal flash polishing time was 0.4–0.6 s.

Annealing was performed by two different methods: (1) in situ annealing for thin foil samples in a high-voltage electron microscope (JEM-ARM1300) where the temperature range was 573–873 K and vacuum level was 5×10^{-6} Pa; (2) furnace annealing for bulk samples in a vacuum condition, where the temperature was 873–1273 K for 15 min. After electro polishing, the particle structures were surveyed by conventional high-resolution microscopy (JEM-2010F).

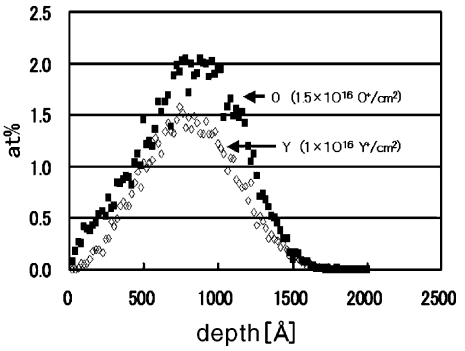

Fig. 1. The calculated distribution of elements after dual ion-implantation of 400 keV Y^+ and 83 keV O^+ to $1.0\times10^{16}/cm^2$ and $1.5\times10^{16}/cm^2$.

3. Results

3.1. Development of particles during in situ annealing

Fig. 2 shows a sequence of particle development in a thin specimen during in situ observation. Before annealing, a small amount of the particles was observed, which means that particle precipitation takes place under the dual ion-implantation condition. Their size was about 5 nm. In Fig. 2(b)–(d), it is clear that additional particles nucleated and grew due to the annealing.

Fig. 3 shows the particle number density and average size as a function of the in situ annealing temperature. No microstructural change occurred till 570 K, but the average size clearly increased with increasing temperature above 570 K. The number density started increasing at 625 K, and at the same time, extra spots developed in the diffraction patterns. Both growth and nucleation continued up to 823 K, after which they saturated. A small decrease in the number density was confirmed at 873 K, which may suggest Ostwald ripening. Fig. 4 shows the dark field image from extra spots after annealing at 873 K. It is confirmed that the particles are distributed homogeneously after growing in size to the several tens of nanometer level. Such a random distribution is much more ideal compared to the particle structure in commercial ODS samples developing during MA.

After in situ annealing, EDS analysis was applied to the particles and the presence of Y was confirmed. Diffraction patterns were also analyzed, we conclude that the particles are Y_2O_3 with BCC structure where the lattice constant is 1.06 nm.

3.2. Particle behavior after bulk annealing

Fig. 5 shows typical particle structures in the specimens after bulk annealing at 873–1273 K for 15 min. Nano-sized particles were observed in all annealed samples, and the particle distribution was as almost homogeneous as that of the thin specimens. However, the size (6.5 nm) and number density (4.4×10^{20} m^{-3}) did not change much as the temperature varied. The size was relatively small and the number density was high compared with in situ annealing of thin specimens (Fig. 6). This suggests that nucleation and growth of the particles starts below 873 K, and continues to higher temperatures side compared with thin specimen. This difference

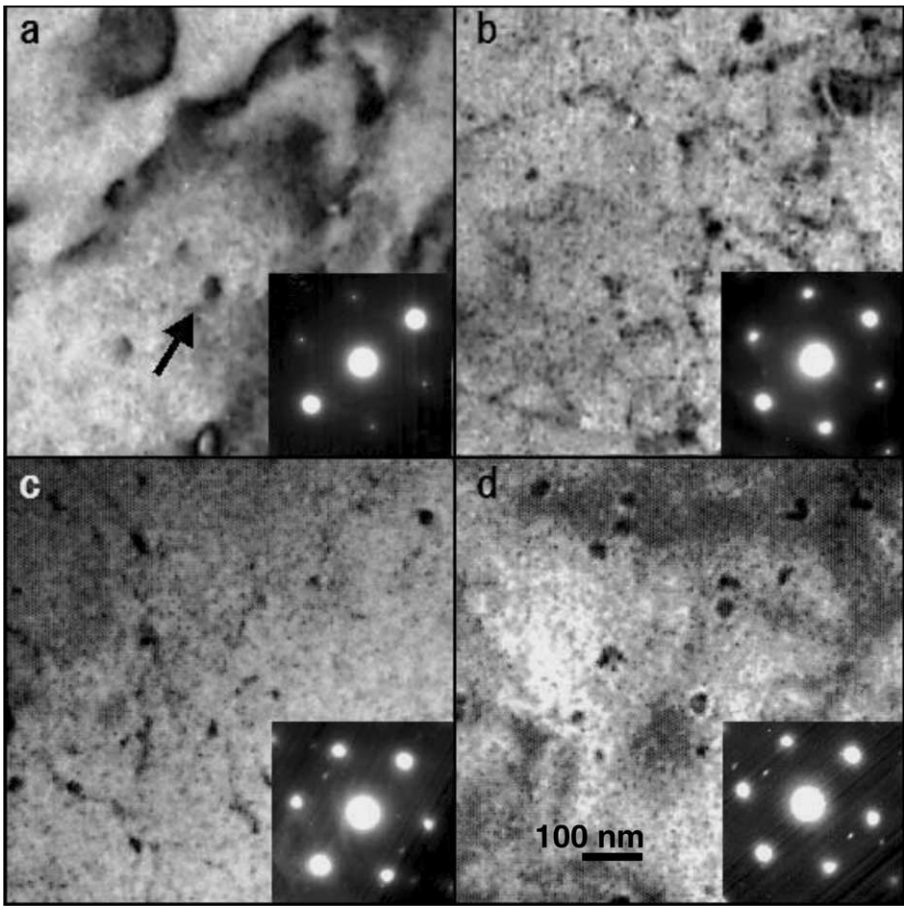

Fig. 2. Nano-oxide particle structure during in situ annealing: (a) before annealing, and annealed at (b) 573 K, (c) 623 K and (d) 673 K.

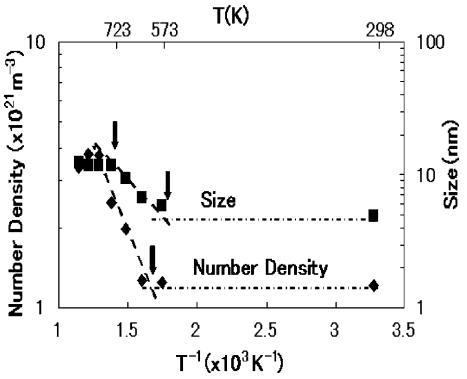

Fig. 3. The particle number density and average size for thin specimens as a function of the in situ annealing temperature.

may be explained by different annealing conditions, such as electron-irradiation enhanced diffusion during in situ observation.

EDS analysis and electron diffraction were carried out, and the particles identified as Y_2O_3 structure as following thin specimen annealing. It was noted that a halo ring and some additional spots in the diffraction pattern come from surface oxides and a film formed during bulk annealing.

4. Discussion

4.1. Solute distribution after dual ion-implantation

In this study a small amount of Y_2O_3, about 0.01% volume fraction, precipitated in the as-implanted condition. The homogeneity of the implanted elements is not perfect, as expected from the TRIM code calculation. It can be concluded that almost all of the implanted elements remained in the matrix in a super-saturated solution, because the volume fraction of precipitate increased up to 0.32% after in situ annealing (Fig. 7). Y_2O_3

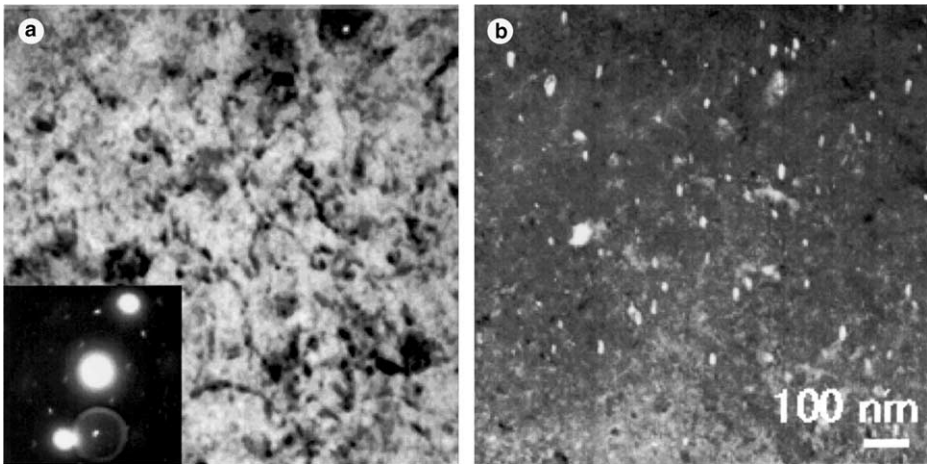

Fig. 4. Nano-oxide particle structure during in situ annealing at 873 K: (a) bright field image, and (b) dark field image.

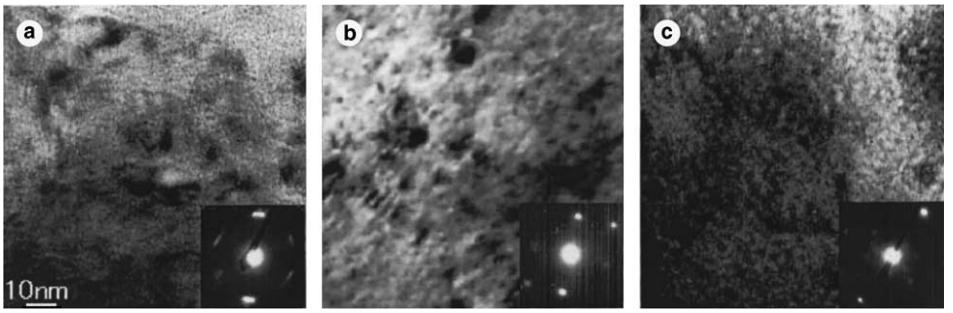

Fig. 5. Nano-oxide particle structure after bulk annealing: annealed at (a) 873 K, (b) 1073 K and (c) 1273 K.

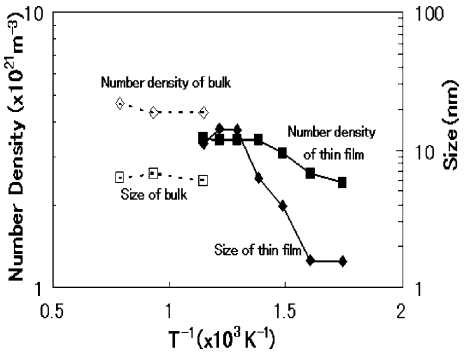

Fig. 6. The particle number density and average size for bulk specimens as a function of annealing temperature.

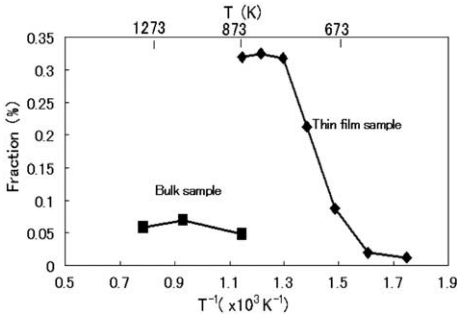

Fig. 7. Volume fraction of the particles as a function of annealing temperature.

did not change until 573 K. At low temperature, it is assumed that diffusion distance is short. This condition can be regarded as a super-saturated solid solution, or forced-solid solution, similar to the MA condition. For explaining the remaining small amount of precipitation, we consider the roles of strong chemical affinity of implanted O and Y, as well as the large amount of

radiation-produced point defects. Both of these may assist the formation of Y_2O_3 nuclei, even at low temperatures. Such factors may be achieved in MA condition, i.e., decomposition of Y_2O_3 due to mechanical grinding, and lattice defects and dislocations with high density. However, MA method cannot achieve the some level of homogeneous atomic mixing obtained with dual ion-implantation.

4.2. Precipitation during in situ annealing

It should be noted that the starting temperature for the growth was relatively low, 573 K, which was extrapolated from the growth rate of the particles. The nano-particles may grow at this temperature due to the assistance of lattice defects with high concentration. On the contrary, the starting temperature for additional nucleation was 673 K, which was extrapolated from the number density line. Super-saturated O and Y can form additional nuclei at relatively high temperature. Both the growth and nucleation processes are completed at 723 K.

The activation energy of the growth was estimated as 0.22–0.29 eV from the extrapolated lines. This energy is relatively small compared with 1.7 eV for diffusion in α-Fe. If the small energy can be assumed to be the diffusion energy, the process appears to be enhanced by the electron-irradiation and the thin film effects. The amounts of irradiation were about 3 dpa during in situ observation. Generally, the thin film effects are carbon contamination and surface diffusion. In this case, there is little influence of carbon contamination, because Y_2O_3 is an oxide. It is assumed that main influence is surface diffusion.

4.3. Comparison of atomic mixing

It has been reported that intensive growth of Y_2O_3, may start from 800–900 K for ODS ferritic steels made by MA [9]. This temperature range is similar to the result of dual ion-implanted samples followed by bulk annealing. However dual ion-implanted thin samples followed by in situ annealing showed growth at lower temperature. This may result from enhanced diffusion due to radiation damage and surface diffusion. The strong enhancement of this precipitation is supported by the large volume fraction of the particles in this sample, which means precipitation even at low temperature.

From the comparison of mixing methods, we can conclude that dual ion-implantation can induce a fine distribution of nano-scale oxide-forming elements under super-saturated condition, and can achieve much finer homogeneity of the nano-scale oxides compared with the MA process.

5. Conclusion

Dual ion-implantation was applied to control nano-scale oxide formation in ferritic steels. Both in situ annealing in an electron microscope for thin samples and conventional annealing for bulk samples were carried out at 300–1300 K. Almost all of the implanted Y and O are in the super-saturated solid solution in the as-implanted condition, which is equivalent to the MA condition. Nano-particles of Y_2O_3 precipitated during annealing, but the starting temperatures for the nucleation and growth depend on the annealing process. In thin specimens the growth of Y_2O_3 started at 573 K, and the nucleation started at 613 K, and this process is saturated at 723 K. The activation energy was about 0.22–0.29 eV, which is relatively small compared with bulk diffusion. This result can be explained by the assistance of irradiation-enhanced diffusion. From the comparison of mixing methods, we can conclude that dual ion-implantation can induce a fine distribution of oxide-forming elements under super-saturated condition on the nano-scale, and can achieve much finer homogeneity of the nano-scale oxides compared with MA.

Acknowledgements

We thank Mr Tanaka, Mr Suda and Professor Watanabe of Hokkaido University for their cooperation in progressing experiments and discussions. Also we thank Dr P.R. Okamoto and Dr N.Q. Lam, ANL, for encouraging this study. This work was partially supported by the US-DOE, Office of Science, under contract W-31-109-EN6-38.

References

[1] S. Yamashita, K. Oka, S. Ohnuki, N. Akasaka, S. Ukai, J. Nucl. Mater. 307–311 (2002) 283.
[2] S. Ukai, T. Nishida, H. Okada, M. Inoue, M. Fujiwara, T. Okuda, K. Asabe, J. Nucl. Sci. Technol. 34 (3) (1997) 256.
[3] S. Ukai, T. Nishida, T. Okuda, T. Yoshitake, J. Nucl. Sci. Technol. 35 (4) (1998) 294.
[4] S. Ukai, M. Harada, H. Okada, M. Inoue, S. Nomura, S. Shikakura, K. Asabe, T. Nishida, M. Fujiwara, J. Nucl. Mater. 204 (1993) 65.
[5] S. Ukai, M. Harada, H. Okada, M. Inoue, S. Nomura, S. Shikakura, T. Nishida, M. Fujiwara, K. Asabe, J. Nucl. Mater. 204 (1993) 74.
[6] J. Saito, T. Suda, S. Yamashita, S. Ohnuki, H. Takahashi, N. Akasaka, M. Nishida, S. Ukai, J. Nucl. Mater. 258–263 (1998) 1264.
[7] S. Ukai, M. Fujiwara, J. Nucl. Mater. 307–311 (2002) 749.
[8] M. Klimiankou, R. Lindau, A. Moslang, J. Cryst. Growth 249 (2003) 381.
[9] T. Okuda, M. Fujiwara, J. Nucl. Sci. Lett. 14 (1995) 1600.